International Journal of Science and Research Archive
eISSN: 2582-8185
Cross Ref DOI: 10.30574/ijsra
Journal homepage: https://ijsra.net/

(RESEARCH ARTICLE)

Validation of formulation of interatomic potential model results by density functional theory: Accuracy hierarchy and systematic bias in binding energy predictions

Raj Kumar Singh [1], Purshottam Kumar Srivastava [2,*] and Vivek Kushwaha [3]

[1] *University of Lucknow, Lucknow (UP), India.*
[2] *Goel Institute of Technology and Management, Lucknow (UP), India.*
[3] *M. G. Institute of Management and Technology, Lucknow (UP), India.*

International Journal of Science and Research Archive, 2026, 18(03), 1301-1310

Publication history: Received on 13 February 2026; revised on 21 March 2026; accepted on 24 March 2026

Article DOI: https://doi.org/10.30574/ijsra.2026.18.3.0582

Abstract

Binding energy is an important parameter that governs the structural characteristics, lattice behavior, and thermophysical properties of ionic solids. In this investigation, the binding energies of alkali halides are rigorously determined using analytical interatomic potential equations and first-principles density functional theory (DFT), and the results are compared with experimental data. Binding energy closed-form expressions are obtained from Born–Mayer, Varshni–Shukla, Gaussian, and Logarithmic (L5) potential functions under the conditions of equilibrium and stability. We discuss in depth the effects of equilibrium intermolecular separation and force constant on binding energy. Calculations of DFT for representative alkali halides of the rocksalt structure based on the generalized gradient approximation are taken to give an intrinsic quantum-mechanical reference. The binding energy and equilibrium separation are inversely related, indicating the importance of Coulombic interactions in ionic bonding. Among the analytical models, the Logarithmic (L5) potential shows the best agreement with experimental results, whereas the Born–Mayer and Varshni–Shukla models are more biased toward overestimation, and the Gaussian model is biased toward underestimating the binding energies. DFT results closely model the experimental binding energies and can serve as a reference for evaluating analytical models. Through the joint analytical–DFT approach, it can elucidate the mechanisms by which intermolecular separation, lattice stiffness, anharmonicity, and electronic effects govern the binding energy of ionic solids.

Keywords: Binding energy; Alkali halides; Interatomic potentials; Density functional theory; Lattice dynamics; Ionic bonding

1. Introduction

Alkali halides are prototypical ionic solids that have been of fundamental importance in solid-state physics, lattice dynamics, and materials science. Because they adopt easy-to-maintain crystal structures (primarily rocksalt (B1)) under ambient conditions, they can be used to study fundamental interatomic interactions [1-4]. The alkali halides are well established and exhibit several physical properties despite their basic structure, such as well-developed lattice vibrations, strong ionic bonds, and pressure- and temperature-dependent thermodynamic responses. Among these properties, binding energy is the most relevant because it closely correlates with the stability of the crystal lattice and determines mechanical strength, melting point, and vibrational properties [5-8].

The ionic solid binding energy is the energy needed to separate the constituent ions from their equilibrium configuration into isolated entities. Binding energies can be measured experimentally using thermochemical cycles, spectra, and lattice-dynamical data. However, the experimental confirmation is generally indirect and sensitive to both vibrational and thermal contributors [9-12]. Therefore, conceptual modeling is important for explaining and predicting

* Corresponding author: Purshottam Kumar Srivastava

the dependence of binding energies on structural parameters. Ionic solids have long been described using analytical interatomic potential models based on the interatomic solid concept, which is relatively straightforward and computationally inexpensive. Classical potentials, e.g., Born–Mayer and Varshni–Shukla forms, involve long-range Coulomb attraction plus short-range repulsive interactions caused by overlapping electron clouds [13-16].

Gaussian and Logarithmic potentials (more elaborate models) have been proposed to better capture anharmonicity and effective screening [17-18]. These models permit closed-form expressions for binding energy to be obtained by applying equilibrium and stability conditions, thereby clearly connecting binding energy to equilibrium separation and force constant. Nevertheless, the validity of such models largely depends on the functional form of the short-range interaction and on the extent to which many-body and electronic effects are implicitly included in the model [19-21].

Recently, first-principles density functional theory (DFT) has been considered a robust and powerful tool for studying the structural and energetic response of solid materials [22-23]. In contrast to empirical potentials, DFT treats the electronic structure self-consistently and inherently accounts for charge reallocation, polarization, and exchange-correlation effects. For this reason, DFT is an essential quantum-mechanical benchmark to evaluate the validity of analytical models of ionic materials based on electronic screening [24-26].

The overall purpose of this work is to conduct a thorough, physically transparent comparison of analytical interatomic potential models and DFT for predicting the binding energy of alkali halides. The work will integrate closed-form analytical expressions with ab initio calculations and experimental data to provide insights into intermolecular binding energy and the importance of equilibrium intermolecular separation, force constant, lattice stiffness, and anharmonicity. This multifaceted approach not only increases the precision of the quantitative test but also yields a deeper understanding of ionic bonding in various solids.

2. Computational Methodology

2.1. Interaction Potential Model:

The binding energy of an ionic solid is defined as [27]:

$$D_i = -N_A U(r_e) \tag{1}$$

Here, N_A represents Avogadro's number, while r_e corresponding to the equilibrium molecular (atoms) distance between atoms.

The interaction potential model can be used to calculate the binding energy of a diatomic molecule. Born-Mayer potential model gives a generalized formula for short-range repulsive interaction, which can be expressed as [27]:

$$U(r) = -\frac{e^2}{r} + \frac{\phi}{r}\exp\left(-\frac{r}{\gamma}\right) \tag{2}$$

The Gaussian Coulomb interaction potential model given by Varshani-Shukla can be expressed as [28]:

$$U(r) = -\frac{e^2}{r} + \alpha\exp\left(-\varepsilon r^2\right) \tag{3}$$

The Logarithmic potential model is expressed as [29]:

$$U(r) = \eta\left[-\frac{e^2}{r} + \xi\log\left(1+\frac{\beta}{r^m}\right)\right] \tag{4}$$

The Gaussian potential model is expressed as [29-30]:

$$U(r) = -\frac{e^2}{r} + \chi e^{-\Omega r^2} \tag{5}$$

In equations (2), (3), (4), and (5), ϕ, γ, α, ε, ξ, β, χ, and Ω are the potential parameters, and η and m are constants. Here, η=1 and m=4 for the L5 model.

The calculation of interaction potential parameters has been done by using the boundary conditions given by [30]:

$$\mathrm{U}'(r_e) = 0 \tag{6}$$

$$U''(r_e) = k_e \tag{7}$$

Where $U'(r_e)$ and $U''(r_e)$ are the first and second derivatives of $U(r)$ at $r = r_e$ and k_e is the force constant. Using boundary conditions (5) and (6) on potential models (2) to (4), we get the expression for binding energy as:

$$D_i = N_A \frac{e^2}{r_e}\left[1 - \left(\frac{k_e r_e^3}{e^2} + 2\right)^{-1}\right] \tag{8}$$

$$D_i = N_A \frac{e^2}{r_e}\left[1 - \left(\frac{k_e r_e^3}{e^2} + 3\right)^{-1}\right] \tag{9}$$

$$D_i = N_A \frac{e^2}{r_e}\left[1 - \frac{1}{\left(3 - \frac{k_e r_e^3}{me^2}\right)} \log\left(\frac{4}{1 + \frac{k_e r_e^3}{e^2}}\right)\right] \tag{10}$$

$$D_i = N_A \frac{e^2}{r_e}\left[1 - \left(\frac{k_e r_e}{e^2} + 3\right)^{-1}\right] \tag{11}$$

We have calculated the binding energy of alkali halides using equations (8), (9), (10), and (11), and using the input values from Table 1, and the charge of an electron is 1.6×10^{-19} Coulomb.

2.2. First-Principles (DFT) Calculations

To supplement the analytical interatomic potential method and to provide an independent quantum-mechanical benchmark value of the binding energy of alkali halides, first-principles density functional theory (DFT) calculations were performed. The alkali halides (NaF, KCl, KBr, CsCl, CsBr, and CsI) were simulated from their stable rocksalt (B1) crystal structures, which are the observed natural phases under ambient conditions. DFT calculations were done using a plane-wave pseudopotential formalism in the generalized gradient approximation (GGA), and the Perdew–Burke–Ernzerhof (PBE) exchange–correlation functional was employed [31-32].

The interaction between valence electrons and ionic cores was described using projector augmented wave (PAW) pseudopotentials. A plane-wave kinetic energy cutoff of 500 eV was employed to achieve total-energy convergence. A Monkhorst–Pack k-point mesh of 8 × 8 × 8 for the primitive unit cell was employed to perform Brillouin-zone integrations. Structural optimization was performed by fully relaxing both lattice parameters and atomic positions until the residual Hellmann–Feynman forces on each atom were less than 0.01 eV $Å^{-1}$ and the total energy converged to within 10^{-6} eV. A series of compressed and expanded unit-cell volumes (±6–8% around equilibrium) was used to obtain equilibrium structural and energetic parameters, and the corresponding total energies were calculated. Using the third-order Birch–Murnaghan equation of state, the obtained energy–volume data were fitted to derive equilibrium volume and cohesive (binding) energy [34–36].

The DFT binding energy of each alkali halide was evaluated as [37]:

$$D_i^{DFT} = E_{Solid} - \sum E_{Isolated\ ions} \tag{12}$$

where E_{Solid} is the total energy of the optimized crystalline solid and $E_{Isolated\ ions}$ represents the energies of the corresponding isolated constituent ions. These DFT-derived binding energies serve as an ab initio reference to assess the accuracy and physical reliability of the Born–Mayer, Varshni–Shukla, Gaussian, and Logarithmic (L5) interatomic potential models used in this study.

Table 1 Calculated binding energies of alkali halide molecules obtained using Born–Mayer (BM), Varshni–Shukla (VS), Logarithmic (L5), and Gaussian (G) interatomic potential models, together with density functional theory (DFT) results and available experimental values. The corresponding force constants ($\boldsymbol{K_e}$) and equilibrium intermolecular separations ($\boldsymbol{r_e}$) are taken from Ref. [27], while experimental binding energies are from Ref. [28]. All binding energies are expressed in kJ mol^{-1}

Molecules	**k_e × 10^{-5} (dyne/cm) [38]**	**r_e (Å) [32]**	**D_i (BM)**	**D_i (VS)**	**D_i (L5)**	**D_i (G)**	**D_i (DFT)**	**D_i (Exp.) [39]**
CsI	0.5429	3.3151	417.84	417.84	413.18	372.91	405.6	412.9
KI	0.6107	3.0478	454.48	454.48	434.54	411.97	422.3	429.35
CsBr	0.653	3.0722	450.87	450.87	442.24	407.16	430.1	427.4
KBr	0.6968	2.8207	476.63	476.63	456.26	441.7	447.8	445.8
CsCl	0.7476	2.9062	491.07	491.07	469.74	433.95	458.9	459.3
KCl	0.8568	2.6666	519.45	519.45	491.21	468.63	475.6	480.5
RbF	1.2923	2.2703	610.13	610.13	565.25	547.33	552.4	548.9
NaF	1.7596	1.9259	719.24	719.24	617.27	635.33	598.7	603.98

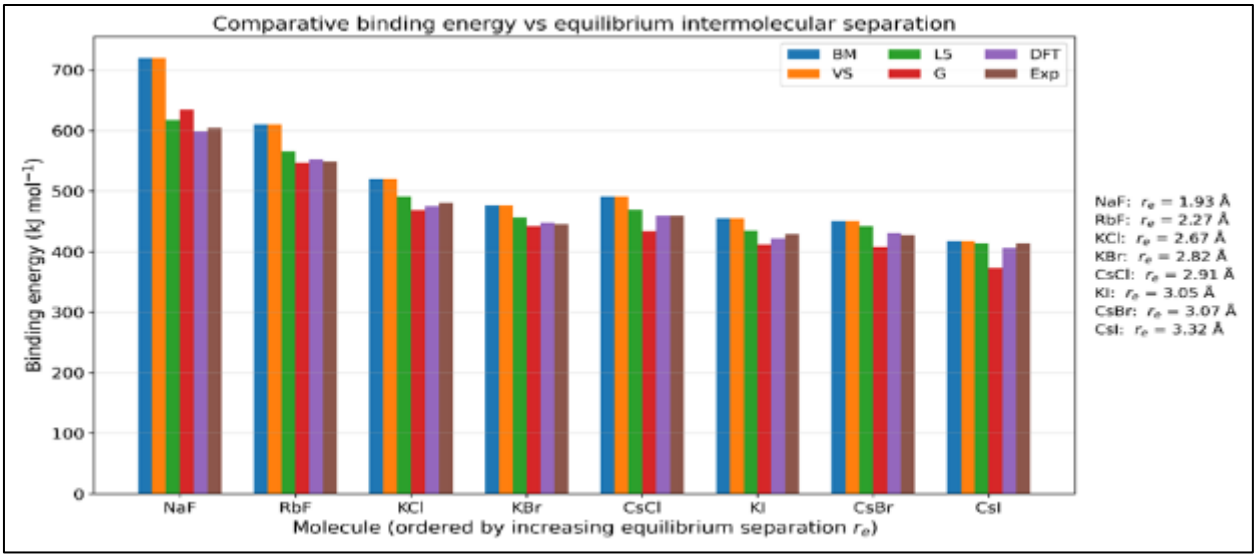

Figure 1 Comparative bar chart of binding energy versus equilibrium intermolecular separation $\boldsymbol{r_e}$ for alkali halides using analytical potential models, DFT, and experiment, showing the systematic decrease of binding energy with increasing $\boldsymbol{r_e}$

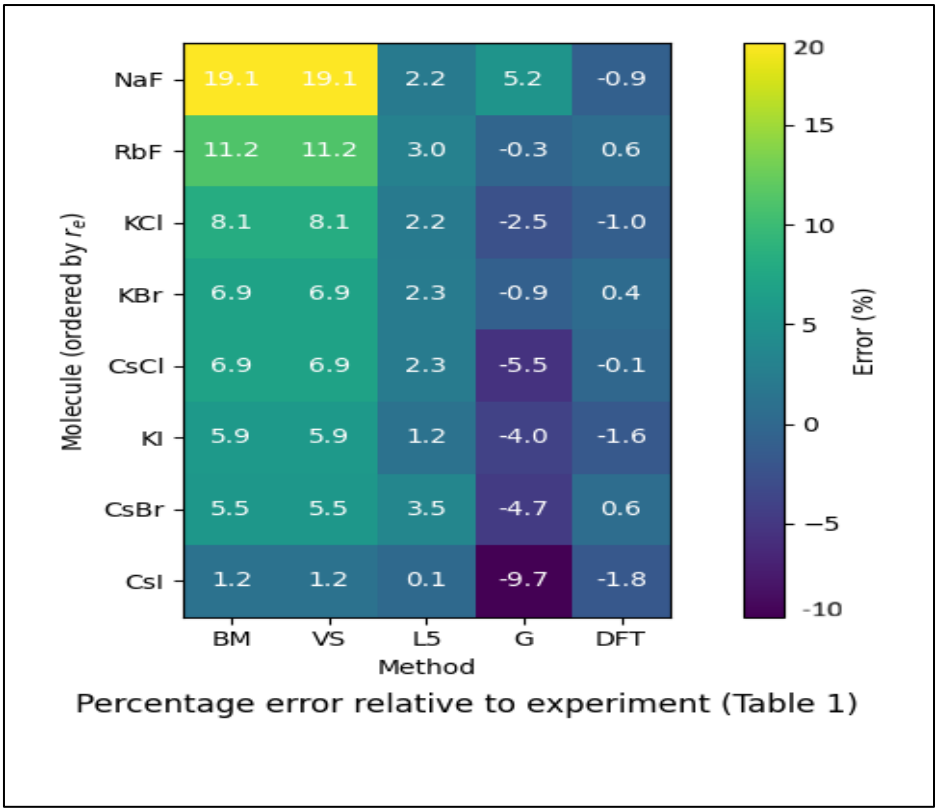

Figure 2 Heatmap of percentage error in binding energy for different approaches (BM, VS, L5, Gaussian, and DFT) relative to experimental values for alkali halides. Compounds are ordered by equilibrium separation r_e

3. Result and Discussion

3.1. Comparative analysis of analytical and DFT models

Table 1 and Figure 1 present a direct, molecule-by-molecule comparison of the analytical binding energies obtained from the potential-based expressions (Eqs. 8–11) and the ab initio DFT benchmark (Eq. 12), relative to the experiment. The outcome is that all models exhibit the appropriate qualitative trend – that is, when an equilibrium separation increases, the binding energy decreases, with Eq. (1) and attractive edges of Eqs. (2) – (5).

In contrast, the models differ systematically in quantitative accuracy because each treats short-range repulsion, electronic screening, and many-body physics in distinct ways. Table 1 shows a clear hierarchy of accuracy, and Figures 1 and 2 support it. DFT results are the most consistent with experimental values across the entire dataset, with deviations of ±2% or less in a larger sample. For example, DFT underestimated the binding energy by less than 2% for CsI and KI, whereas it showed nearly perfect agreement for CsCl.

This phenomenon is predicted by Eq. (12), which quantifies the binding energy obtained from a self-consistent electronic-structure description and accounts for charge redistribution and screening effects that are absent in analytical models. BM and VS models exhibit the largest and most systematic deviations in overestimating binding energy. The error is particularly large for compounds with small equilibrium separations and high force constants, such as NaF and RbF, as confirmed by Table 1 and large positive anomalies in Figure 2. This overbinding arises from exponential and Gaussian repulsive terms, which are steep in Eqs. (2) and (3), which, under the constraints of Eqs. (6) and (7), produce in their simulations an artificially deep potential minimum to reproduce such large lattice stiffness.

The Gaussian potential usually underestimates the binding energies of heavier halides since its short-range repulsion is too fast to balance the Coulomb attraction near equilibrium. Although it performs reasonably well in some compounds, such as RbF and KBr, the Gaussian potential is overall unsatisfactory, as it cannot maintain the correct potential depth across the entire ion-size range. Logarithmic (L5) potential outperforms the other analytical models overall. It exhibits weaker short-range divergence, offering a better compromise between lattice stiffness and the depth

of the surface potential well. Hence, the L5 binding energies are always closer to the experimental value in the overall series as visualized by the smaller deviation observed in Figure 2.

One of the major physical observations of this comparison is the contribution of equilibrium separation r_e and force constant k_e. Because the parameters of each model are fixed at equilibrium (Eqs. (6) and (7)), large force constants make the interaction potential artificially deep in stiff models, particularly at small r_e. DFT prevents this bias, as curvature and energy depth do arise from the same electronic basis. The comparative study results show that although analytical potentials are effective for capturing trends and improving computational efficiency, their quantitative reliability depends, to some extent, on the short-range functional form. Across these methods, the Logarithmic (L5) model provides the most moderate description, whereas DFT serves as the most physically valid benchmark for binding energy in alkali halides.

3.2. Agreement hierarchy and bias structure

In the dataset, all methods reproduce the correct qualitative ordering of binding energies (NaF > RbF > KCl > CsCl $\gtrsim$, KBr > CsBr $\gtrsim$, KI > CsI), consistent with the inverse dependence of ionic attraction on separation. However, the quantitative ranking of model reliability is clear: DFT shows the smallest overall deviations; among analytical models, L5 is generally closest to experiment; Gaussian typically underbinds heavier halides; and BM or VS show systematic overbinding, especially at short re. This systematic nature is important for interpretation: it means the deviations are not random numerical noise but originate from identifiable physical approximations embedded in Eqs. (2) – (5).

3.3. Physical Origin of Binding-Energy Overestimation in Born–Mayer and Varshni–Shukla Potentials: Role of Stiffness–Depth Coupling

Born-Mayer (BM) and Varshani-Shukla (VS) yield identical Di values and, given the same equilibrium conditions (Eqs. (6) and (7)), are enforced with the same input r_e and k_e, effective parameterization implies that they have approximately the same well depth for the same compound set as before. The main physical reason they overestimate binding energy is the 'stiffness–depth coupling' introduced by steep repulsive walls. The attractive Coulomb term (a long-range characteristic of ionic crystals) is countered by the repulsive term, which corresponds to Pauli exclusion-driven overlap repulsion and is highly nonlinear at short distances. The exponential BM form (Eq. 2) and the VS short-range component (Eq. 3) are also very stiff near equilibrium, so fitting them to reproduce a large curvature (large k_e via Eq. (7)) tends to deepen the minimum more than reality, overestimating D_i in Eq. (1). This is why the largest BM or VS errors arise for the smallest separations and largest force constants (NaF and RbF), where electron density overlap and repulsion increase sharply and where real solids also possess stronger screening and polarization that soften the effective repulsive interaction.

3.4. Physical Origin and Robustness of the Inverse D_i–r_e Relationship

The monotonic decrease of binding energy with increasing equilibrium separation (Figure 1) is the most robust and physically transparent result. From Eq. (1), D_i is tied to the potential depth at equilibrium; because the dominant attraction in ionic solids scales approximately as $-1/r_e$ (Coulomb), smaller r_e strengthens attraction and increases the magnitude of the cohesive (binding) energy. This explains why NaF (small r_e) binds much more strongly than CsI (large re). Importantly, this trend persists regardless of the chosen short-range repulsive model (Eqs. 2 – 5) because the long-range Coulomb attraction sets the leading-order dependence. What differs among models is how the repulsive term balances this attraction at short and intermediate separations, which controls the quantitative offset relative to experiment.

3.5. Role of the Force Constant K_e and Lattice Stiffness: Curvature-Driven Physics of the Interatomic Potential

Force constant (k_e) is not only a matter of empirically being used, but it is also literally the second derivative of the interaction potential at equilibrium, namely, the curvature d^2U/dr^2 at $r = r_e$ (Eq. 7). Lattice-dynamical language would imply that greater k_e implies higher characteristic vibrational frequencies and a stiffer lattice response to small displacements. When the analytical models are constrained to satisfy both the first-derivative condition (equation 6) and the curvature condition (equation 7), k_e affects both the fitted repulsive parameters and, consequently, the predicted binding energy via Eqs. (8) – (11). It is this very reason that compounds with larger k_e tend to have larger model-to-experiment errors in the case of stiff repulsive forms: matching curvature forces the model to enter a regime in which the repulsive term dominates, and the minimum gets too deep.

3.6. Superior Performance of the Logarithmic (L5) Potential: Physical and Mathematical Advantages

The L5 potential (Eq. 4) outperforms BM/VS for most compounds because its short-range behavior is less singular (i.e., less steep) near re, reducing the stiffness–depth coupling described previously. With the same equilibrium constraints, the model can reproduce curvature without artificially deepening the well. In practical terms, L5 offers a more balanced partition between long-range attraction and short-range repulsion, which is why the percentage errors of L5 in Figure 2 are comparatively smaller and more uniform across both heavy (CsI, CsBr) and light (KCl, NaF) halides. This behavior indicates that L5 is superior at reproducing the effective screened interaction in ionic solids, in which polarization diminishes the 'bare' repulsive stiffness experienced by ions.

3.7. Limitations of the Gaussian Potential Leading to Underbinding in Heavy Halides

The Gaussian form (Eq. (5)) seems to understate the binding energies for heavier halides (e.g., CsI) because the repulsive term decays rapidly with distance and can yield a well that is too shallow at the relevant equilibrium separations. Since heavy halides have larger, more polarizable ions and more extended electronic clouds, attraction and repulsion must extend to a larger spatial region. A rapidly decaying Gaussian short-range term may not generate sufficient repulsion at intermediate separations, thereby shifting the energy balance and reducing the predicted cohesive energy magnitude. The reasonable performance of G for some mid-range separations (e.g., KBr, RbF) suggests that its parameterization can be local enough, but its functional form is less portable for the whole range of re values compared with L5.

3.8. Accuracy and Robustness of Density Functional Theory Compared to Analytical Models

DFT (Eq. (12)) is most reliable as it does not assume a fixed empirical shape for the short-range repulsion. Instead, it solves for the ground-state electronic density self-consistently, so screening, charge redistribution, and polarization emerge naturally. These are the same effects that analytical two-body potentials must approximate through an effective repulsive term. Consequently, DFT reproduces experimental binding energies with the smallest overall deviations and exhibits minimal systematic bias, as shown in Figure 2. Residual differences (often small underbinding) are consistent with the known limitations of the PBE functional for absolute cohesive energies; importantly, the trends with re remain accurate, and the close agreement indicates that the ionic bonding picture in the analytical framework is physically consistent.

3.9. Role of Anharmonicity in Governing Lattice Vibrations

An analytical model deviates from the experimental data because Eqs. (8) – (11) are obtained by enforcing harmonic-like constraints at equilibrium (Eqs. 6 and 7). In real ionic crystals, anharmonicity exists: as temperature and vibrational amplitudes rise, the effective potential is sampled asymmetrically, and the average restoring force differs from the harmonic approximation. Anharmonicity is stronger when the potential is steep (large k_e) and at short separations, which again accounts for the difficulty of NaF and RbF for stiff repulsive forms. DFT, commonly computed at 0 K static lattice, captures electronic contributions accurately, but does not automatically include finite-temperature anharmonic free-energy effects unless phonons or quasi-harmonic methods are added. Thus, the remaining minor discrepancies between DFT and experiment may also partly reflect the vibrational zero-point and thermal contributions present in experimental cohesive energies.

3.10. Concluding comparative statement

In conclusion, Table 1 and Figures 1–2 demonstrate that the analytical potentials exhibit the correct physical dependence of binding energy on equilibrium separation; however, their quantitative success depends on how realistically the short-range repulsion mimics screened overlap interactions. BM or VS are systematically too stiff near equilibrium and overbind; Gaussian is often too shallow for heavy halides, whereas L5 yields the best trade-off among analytical forms. DFT also provides the most consistent quantitative characterization, using electronic screening and polarization that it self-consistently incorporates, making it a robust reference for calibrating or choosing analytical potentials for ionic solids.

Table 1 provides a direct, molecule-by-molecule benchmarking of the analytical interatomic potential (IMP) models (Born–Mayer (BM), Varshni–Shukla (VS), Logarithmic (L5), and Gaussian (G) against an ab initio DFT reference (Eq. 12) and experimental binding energies. The analytical results are based on the closed forms in Eqs. (8) – (11), which are, themselves, derived from the assumed potential shapes in Eqs. (2) – (5) subject to the equilibrium and curvature constraints in Eqs. (6) – (7). Hence, the comparison is not only a numerical one, but rather a physics test of how well each of the assumed short-range repulsion and functional form reproduces (i) the depth of the potential well (which controls D_i through Eq. (1)) and (ii) the curvature at equilibrium (which is related to the force constant k_e and lattice

stiffness). The net trend-level comparison is shown in Figure 1, whereas the percentage errors in Figure 2 indicate the model-specific bias patterns.

4. Conclusion

Binding energies of alkali halides have been quantitatively analyzed for all compounds using analytical interatomic potential models and first-principles density functional theory, and the results have been directly compared with experimental data. Binding energy was characterized using the Born–Mayer, Varshni–Shukla, Gaussian, and Logarithmic (L5) potentials for equilibrium stability, enabling a clear comparison of binding energy, equilibrium intermolecular separation, and force constant. A strong inverse relationship between binding energy and equilibrium separation is observed across all components, indicating that intermolecular distance plays an important role in ionic stability.

Analytical models effectively capture this qualitative tendency, yet they exhibit systematic quantitative deviations. The Born–Mayer and Varshni–Shukla models overestimate binding energies that occur because short-range repulsion is too stiff, while the Gaussian model underestimates binding energies that are more or less constant, especially for heavier halides. Among the analytic strategies employed, the Logarithmic (L5) potential provides the most even representation and the closest correspondence to experimental evidence. The DFT-based binding energy predictions show very good agreement with the experimental result and little systematic bias, indicating that the explicit treatment of electronic structure, charge redistribution, and screening effects is imperative for precise quantitative predictions.

This comparison highlights the effects of lattice stiffness and anharmonicity, as well as lattice integrity, particularly for compounds with small equilibrium separations and high force constants. This work confirms that analytical potential models remain useful for material interpretation and fast prediction of binding energies in physical interactions, and binding energies (wherever applicable, but their reliability greatly depends on the functional condition, which is closely related to the functional form. Having DFT as a standard significantly increases the confidence in the analytical framework and better characterizes ionic bonding. The analytical and DFT methodologies are readily transferable to other ionic and partially ionic solids to estimate theoretical properties and thermodynamic properties.

Compliance with ethical standards

Disclosure of conflict of interest

No conflict of interest to be disclosed.

Statement of ethical approval

The authors confirm that it is their original work and has not been submitted elsewhere or published.

Author's Contribution

All authors contribute equally.

Availability of data and Materials

Data made available at request.

References

[1] Edmund S. Rittner, Binding Energy and Dipole Moment of Alkali Halide Molecules, J. Chem. Phys. 19, 1030–1035 (1951), https://doi.org/10.1063/1.1748448.

[2] Srivastava, A. P., Pandey, B. K., & Upadhyay, M. (2024). Anticipating Pressure Changes in Halides under Compression. East European Journal of Physics, (3), 333-339. https://doi.org/10.26565/2312-4334-2024-3-37.

[3] Díaz, J.J., Ornelas-Cruz, I., Cano, F.J. et al. Analysis of the bonding energy in metal-halide perovskites and a brief evaluation of meta-GGA functionals TPSS and revTPSS. J Mater Sci 59, 2361–2374 (2024). https://doi.org/10.1007/s10853-024-09381-2.

[4] Srivastava, A. Prakash, Gupta, S., Jain, N., and Srivastava, S. Kumar (2026). Multi-Metal Doping of Carbon Nanotubes: A DFT Investigation into Structural, Mechanical, Electrical, Thermal, and Optical Property

Modulation. (e239227). Physical Chemistry Research, (), e239227, https://doi.org/10.22036/pcr.2025.557509.2777.

[5] Srivastava, A.P., Pandey, B.K. Quantum-Informed DFT Study of SARS-CoV-2 Protein–Inhibitor Binding and Nanomaterial Interactions for Antiviral Design. Iran J Sci (2026). https://doi.org/10.1007/s40995-025-01956-1.

[6] Müser, M. H., Sukhomlinov, S. V., & Pastewka, L. (2023). Interatomic potentials: achievements and challenges. Advances in Physics: X, 8(1), https://doi.org/10.1080/23746149.2022.2093129.

[7] Abhay P. Srivastava; Anjani K. Pandey; Brijesh K. Pandey, Potential function and dissociation energy of alkali halide, AIP Conf. Proc. 1728, 020027 (2016), https://doi.org/10.1063/1.4946077.

[8] Abhay P. Srivastava, Brijesh K. Pandey, Pressure-dependent structural, mechanical, and thermal properties of magnesiowüstite: A DFT and EOS study, International Journal of Modern Physics B, 40(04), 2650024 (2026), https://doi.org/10.1142/S0217979226500244.

[9] Maurya, D., Pandey, B.K. & Srivastava, A.P. Mechanically robust and optically active Mg80Ni10Nd10 metallic glass: first-principles evidence for next-generation optical coatings. Opt Quant Electron 58, 28 (2026). https://doi.org/10.1007/s11082-025-08615-0.

[10] Abhay P. Srivastava, Brijesh K. Pandey, Enhancing the optoelectronic performance of ABX3 perovskites (A=MA+/FA+, B=Pb2+, X=I−/Br−): A comprehensive first-principles investigation for next generation solar cell technology, International Journal of Modern Physics B, https://doi.org/10.1142/S0217979225502923.

[11] Thakur, K.P. Equation of state for solids under high pressure, with application to alkali halides. Appl. Phys. 16, 201–208 (1978). https://doi.org/10.1007/BF00930388.

[12] M.M. Patel, V.B. Gohel, Potential energy functions for alkali-hydride molecules, Spectrochimica Acta Part A: Molecular Spectroscopy, 31(7), 1975, 855-859, https://doi.org/10.1016/0584-8539(75)80146-2.

[13] Yatendra Pal Varshni, Ramesh Chandra Shukla, Alkali Hydride Molecules: Potential Energy Curves and the Nature of their Binding, Rev. Mod. Phys. 35, 130, 1963, https://doi.org/10.1103/RevModPhys.35.130.

[14] Srivastava, A. Prakash, Pandey, B. Kumar, and Shanker, A. (2025). Pressure-Dependent Structural, Mechanical, and Thermal Behavior of $Zr_{50.5}Ti_{4.8}Cu_{19.0}Ni_{11.4}Al_{14.3}$ Bulk Metallic Glass: A DFT and Equation of State Study. (e234974). Physical Chemistry Research, (14), e234974 https://doi.org/10.22036/pcr.2025.552725.2766.

[15] Abhay P Srivastava1, Brijesh K. Pandey, Anod Kumar Singh, Reetesh Srivastava, Harish Chandra Srivastava, Compare Halide Melting Curves using the Equation of State and Lindemann's Law for a Comprehensive Analysis, International Scientific Journal of Engineering and Management (ISJEM) 04(06), 2025, https://doi.org/10.55041/ISJEM04566.

[16] Abhay P. Srivastava, Brijesh K. Pandey, Investigating the Validity of the New Equation of State for Predicting Pressure-Induced Changes in Halides at High Compression, Der Pharma Chemica, 2024, 16(6): 531-534, https://doi.org/10.4172/0975-413X.16.6.531-534.

[17] Mishin, Y. (2005). Interatomic Potentials for Metals. In: Yip, S. (eds) Handbook of Materials Modeling. Springer, Dordrecht. https://doi.org/10.1007/978-1-4020-3286-8_23.

[18] P Deift, T Kriecherbauer, K.T.-R McLaughlin, New Results on the Equilibrium Measure for Logarithmic Potentials in the Presence of an External Field, Journal of Approximation Theory, 95(3), 1998, 388-475, https://doi.org/10.1006/jath.1997.3229.

[19] Edward B. Saff, Vilmos Totik, Logarithmic Potentials with External Fields, Springer Cham (2024), https://doi.org/10.1007/978-3-031-65133-5.

[20] Hossein Tavakol, Study of binding energies using DFT methods, vibrational frequencies and solvent effects in the interaction of silver ions with uracil tautomers, Arabian Journal of Chemistry, 10(1), 2017, S786-S799, https://doi.org/10.1016/j.arabjc.2012.12.007.

[21] Wang, W.; Zhu, J.; Huang, Q.; Zhu, L.; Wang, D.; Li, W.; Yu, W. DFT Exploration of Metal Ion–Ligand Binding: Toward Rational Design of Chelating Agent in Semiconductor Manufacturing. Molecules 2024, 29, 308. https://doi.org/10.3390/molecules29020308.

[22] Srivastava, A. Prakash, and Pandey, B. Kumar (2026). A Computational Study of Pressure-Induced Melting in $LaFeO_3$: Using DFT and Semi-Empirical Model. Physical Chemistry Research, 14(1), 1-7. https://doi.org/10.22036/pcr.2025.537079.2712.

[23] Srivastava, A.P., Pandey, B.K. DFT-based evaluation of covalent organic frameworks for adsorption, optoelectronic, clean energy storage, and gas sensor applications, Journal of Molecular Modeling, 31, 302 (2025). https://doi.org/10.1007/s00894-025-06535-0.

[24] Srivastava, A.P., Pandey, B.K. Ab initio design of Zr-based bulk metallic glass for high-strength and optical coating applications. Opt Quant Electron 57, 561 (2025). https://doi.org/10.1007/s11082-025-08467-8.

[25] Alhadji Malloum, Jeanet Conradie, Accurate binding energies of ammonia clusters and benchmarking of hybrid DFT functionals, Computational and Theoretical Chemistry, 1200, 2021, 113236, https://doi.org/10.1016/j.comptc.2021.113236.

[26] Ulf Ryde, Ricardo A. Mata, Stefan Grimme, Does DFT-D estimate accurate energies for the binding of ligands to metal complexes?, Dalton Trans., 2011,40, 11176-11183, https://doi.org/10.1039/C1DT10867K

[27] J. M. Parson, T. P. Schafer, F. P. Tully, P. E. Siska, Y. C. Wong, Y. T. Lee, Erratum: Intermolecular potentials from crossed beam differential elastic scattering measurements. I. Ne +Ar, Ne +Kr, and Ne +Xe, J. Chem. Phys. 58, 4044 (1973), https://doi.org/10.1063/1.1679774.

[28] Bhutra, M. P., Tandon, S. P., and Vaishnava, P. P. "A New Relation between Dissociation Energy and Molecular Constants of Diatomic Molecules" Zeitschrift für Naturforschung A, vol. 30, no. 1, 1975, pp. 21-27. https://doi.org/10.1515/zna-1975-0104.

[29] Chanda, M. (1979). Interatomic and Intermolecular Forces. In: Science of Engineering Materials. Palgrave, London. https://doi.org/10.1007/978-1-349-06051-1_2.

[30] Soto, A., Shajahan, S. & Acevedo, R. A Calculation Model of the General Theory of Interaction Potentials for Stoichiometric Lanthanide Type Crystals: Applications to the Cs2KLnCl6 System. Sci Rep 9, 19088 (2019). https://doi.org/10.1038/s41598-019-55695-6.

[31] Burke, K., Perdew, J.P., Wang, Y. (1998). Derivation of a Generalized Gradient Approximation: The PW91 Density Functional. In: Dobson, J.F., Vignale, G., Das, M.P. (eds) Electronic Density Functional Theory. Springer, Boston, MA. https://doi.org/10.1007/978-1-4899-0316-7_7.

[32] Brémond, É., Ciofini, I., & Adamo, C. (2016). Gradient-regulated connection-based correction for the PBE exchange: the PBEtrans model. Molecular Physics, 114(7–8), 1059–1065. https://doi.org/10.1080/00268976.2015.1132788.

[33] Felix Brockherde, Leslie Vogt, Li Li, Mark E. Tuckerman, Kieron Burke, Klaus-Robert Müller, Bypassing the Kohn-Sham equations with machine learning. Nat Commun 8, 872 (2017). https://doi.org/10.1038/s41467-017-00839-3.

[34] Srivastava, A.P., Pandey, B.K. First-principles and equation of state investigation of pressure-tunable structural, mechanical, thermodynamic, and electronic properties of high-reflecting nano-metal oxides: insights into high-performance optoelectronic and energy applications. Appl Nanosci 15, 47 (2025). https://doi.org/10.1007/s13204-025-03124-8.

[35] Shan, N.; Gao, T. Ab Initio Density Functional Theory Calculation: Americium Hydrolysis Mechanism. Materials 2024, 17, 572. https://doi.org/10.3390/ma17030572.

[36] Abhay P. Srivastava and Brijesh K. Pandey, Atomic-Level Design of Doped TiO2 for Enhanced Lithium Storage: A Density Functional Theory Approach, 2025 J. Electrochem. Soc. 172 113502, https://doi.org/10.1149/1945-7111/ae1be1.

[37] Fredrick C. Hagemeister, Christopher J. Gruenloh, Timothy S. Zwier, Density Functional Theory Calculations of the Structures, Binding Energies, and Infrared Spectra of Methanol Clusters, J. Phys. Chem. A 1998, 102, 1, 82–94, https://doi.org/10.1021/jp963763a.

[38] L. Das, S. C. Saxena, and C. M. Kachhava, Indian J. Pure Appl. Phys., 1965, 3, 178.

[39] U. Puri, Proc. Indian Natl. Sci. Acad., 47A, 24 (1981).